

GT2011-45\* ( (

## FATIGUE-LIFE PREDICTION METHOD BASED ON SMALL-CRACK THEORY IN AN ENGINE MATERIAL

**James C. Newman, Jr.**  
Mississippi State University  
Mississippi State, MS, USA 39762  
j.c.newman.jr@ae.msstate.edu

**Balkrishna S. Annigeri**  
Pratt & Whitney  
East Hartford, CT, USA 06118  
balkrishna.annigeri@pw.utc.com

### ABSTRACT

Plasticity effects and crack-closure modeling of small fatigue cracks were used on a Ti-6Al-4V alloy to calculate fatigue lives under various constant-amplitude loading conditions (negative to positive stress ratios, R) on notched and un-notched specimens. Fatigue test data came from a high-cycle-fatigue study by the U.S. Air Force and a metallic materials properties handbook. A crack-closure model with a cyclic-plastic-zone-corrected effective stress-intensity factor range and equivalent-initial-flaw-sizes (EIFS) were used to calculate fatigue lives using only crack-growth-rate data. For un-notched specimens, EIFS values were 25- $\mu\text{m}$ ; while for notched specimens, the EIFS values ranged from 6 to 12  $\mu\text{m}$  for positive stress ratios and 25- $\mu\text{m}$  for R = -1 loading. Calculated fatigue lives under a wide-range of constant-amplitude loading conditions agreed fairly well with the test data from low- to high-cycle fatigue conditions.

### INTRODUCTION

The observation that small or short fatigue cracks can grow more rapidly than those predicted by linear-elastic fracture mechanics (LEFM) based on large-crack data, and grow at  $\Delta K$  levels well below the large-crack threshold, has attracted considerable attention (1-5). Some consensus is emerging on crack dimensions, mechanisms, and possible methods to correlate and to predict small-crack behavior. A useful classification of small cracks has been made by Ritchie and Lankford (6). Naturally-occurring (three-dimensional) small cracks, often approaching microstructural dimensions, are largely affected by crack shape (surface or corner cracks), enhanced crack-tip plastic strains due to micro-plasticity, local arrest at grain boundaries, and the lack of crack closure in the early stages of growth.

Research on small-crack behavior and improved analysis methods have shown that fatigue is "crack propagation" from

microstructural discontinuities in a number of engineered materials, such as aluminum alloys, titanium alloys and steels (7-11). Large-crack thresholds ( $\Delta K_{th}$ ) on a wide class of materials may also be inadvertently too high and crack-growth rates too low in the near-threshold regime due to the load-shedding test method used to generate these data (12-14). New threshold test methods are being developed with compression precracking (15, 16) to generate crack-growth-rate data at very low initial stress-intensity factors with minimal load-history effects. But small-crack data should be generated on these materials to validate the fatigue-life prediction methods based on crack growth from microstructural flaw sizes.

In the present paper, plasticity effects and crack-closure modeling of small fatigue cracks were used on a Ti-6Al-4V titanium alloy to calculate fatigue lives under various constant-amplitude loading conditions (negative to positive stress ratios, R) on notched and un-notched specimens. Fatigue test data came from a high-cycle-fatigue program by the U.S. Air Force (17-21) and the Metallic Materials Properties Development Standards (MMPDS) Handbook (22). A crack-closure model with a cyclic-plastic-zone-corrected effective stress-intensity factor range and equivalent-initial-flaw-sizes (EIFS) were used to calculate fatigue lives using only crack-growth-rate data.

### NOMENCLATURE

a	crack depth measured in thickness direction
$a_i$	initial crack depth
B	thickness
c	crack half-length measure in width direction
$c_i$	initial crack half-length
D	specimen, circular-hole or notch diameter
E	modulus of elasticity
$h_n$	void (or crack) half-height
J	path-independent integral around crack tip
$K_{Ic}$	elastic fracture toughness

$K_J$	stress-intensity factor computed from J-integral
$K_o$	crack-opening stress-intensity factor
$K_{max}$	maximum stress-intensity factor
$K_p$	plastic-zone corrected stress-intensity factor
$K_T$	elastic stress-concentration factor
$N_f$	cycles to failure
$R$	stress ratio ( $S_{min}/S_{max}$ )
$S$	applied stress
$S_{max}$	maximum applied stress
$S_{min}$	minimum applied stress
$S_o$	crack-opening stress
$w$	specimen width
$\alpha$	constraint factor
$\Delta J_{eff}$	effective J-integral
$\Delta K$	stress-intensity factor range
$\Delta K_{eff}$	effective stress-intensity factor range
$(\Delta K_{eff})_T$	effective stress-intensity factor at transition from plane-strain to plane-stress conditions
$(\Delta K_{eff})_{th}$	effective stress-intensity factor range threshold
$(\Delta K_p)_{eff}$	cyclic-plastic-zone corrected effective stress-intensity factor range
$\Delta K_{th}$	threshold stress-intensity factor range
$\rho$	plastic-zone size
$\sigma_o$	flow stress (average yield and ultimate)
$\sigma_{ys}$	yield (0.2% offset) stress
$\sigma_u$	ultimate tensile strength
$\omega$	cyclic plastic-zone size

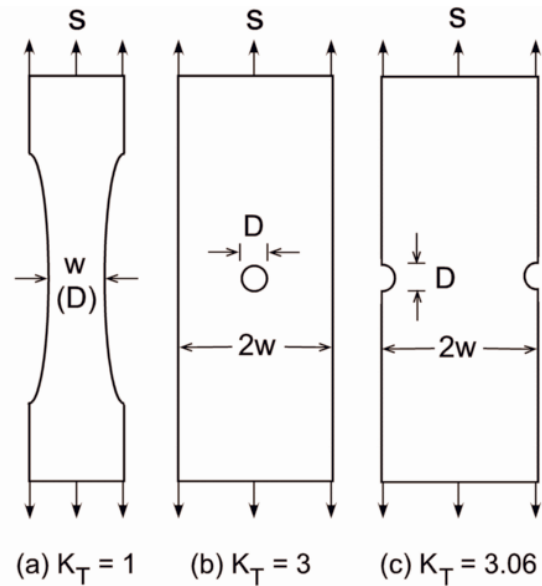


Figure 1. Fatigue specimens analyzed.

### ASTM LOAD-REDUCTION AND COMPRESSION PRECRACKING BEHAVIOR

Currently, in North America, the threshold crack-growth regime is experimentally defined by using ASTM Standard E647, which has been shown in many cases to exhibit anomalies due to the load-reduction (LR) test method. The test method has been shown to induce remote closure, which prematurely slows down crack growth and produces an abnormally high threshold. The fatigue-crack growth rate properties in the threshold and near-threshold regimes for the titanium alloy were obtained from Ref. 13, which used both the LR test method and an improved test method. The improved test method used “compression-compression” precracking, as developed by Suresh (15), Pippin et al (16) and others (12-14), to provide fatigue-crack-growth rate data under constant-amplitude loading in the near-threshold regime, without load-history effects. Test data were obtained from Ref. 13 over a wide range in stress ratios ( $R = 0.1$  to  $0.7$ ) on compact C(T) specimens for three different widths (25, 51 and 76-mm) to help determine the  $\Delta K_{eff}$ -rate relation for large cracks.

The test data at  $R = 0.1$  for the ASTM LR method are shown in Fig. 2(a). These data show a “fanning out” of data at lower growth rates as a function of specimen width ( $w$ ). These results were very similar to those presented by Garr and Hresko (23) on Inconel-718, which showed a width effect on threshold behavior using the ASTM LR method. The 51-mm wide tests produced a lower threshold and faster rates at a given  $\Delta K$  value than the 76-mm wide specimens. The solid curve is a predicted curve based on the  $R = 0.7$  data (as the  $\Delta K_{eff}$ -rate curve) using the crack-closure model (24) with a constraint factor ( $\alpha$ ) of 2. This curve also shows that the 51- and 76-mm specimens produced data far from their expected trend (solid curve).

### MATERIAL AND SPECIMEN CONFIGURATIONS

The titanium alloy considered herein is from the United States Air Force High-Cycle-Fatigue (HCF) program (17-21), that was in the solution treated and over-aged (STOA) condition. The forging, heat-treatment and aging process resulted in a microstructure with an average grain size of 20  $\mu\text{m}$ . The yield stress ( $\sigma_{ys}$ ) was 931 MPa, the ultimate tensile strength ( $\sigma_u$ ) was 979 MPa, and the modulus of elasticity ( $E$ ) was 116 GPa. Additional fatigue data was obtained from MMPDS (22) on an STOA titanium alloy of slightly higher strength.

The large-crack  $\Delta K$ -rate data for the titanium alloy was obtained from C(T) specimens (13) using material obtained from the same batch of material as used in the HCF test program. The fatigue specimens analyzed are shown in Fig. 1. They were: (a) uniform stress ( $K_T = 1$ ) un-notched specimen in a flat sheet or rod form, (b) circular-hole ( $K_T = 3.0$ ) specimen in a flat sheet, and (c) double-edge-notch tension ( $K_T = 3.06$ ) in plate form. All specimens were chemically polished to remove a small layer of disturbed material, which may have contained some machining residual stresses. Here the stress concentration factor,  $K_T$ , is expressed in terms of remote (gross) stress,  $S$ , instead of the net-section stress.

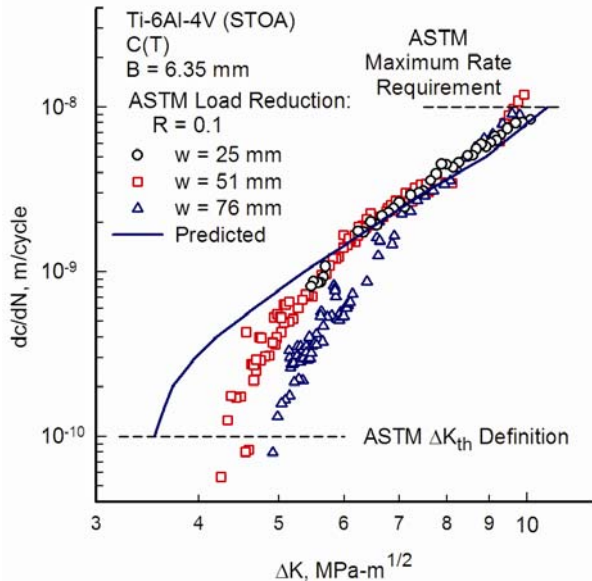


**Figure 2(a). Fatigue-crack-growth-rate data using the ASTM load-reduction test method.**

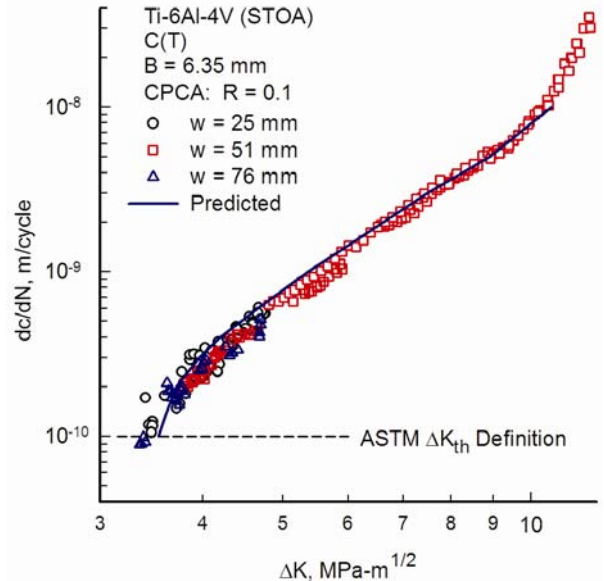


**Figure 2(b). Fatigue-crack-growth-rate data using the CPCA test method.**

In contrast, data from the three specimen widths for  $R = 0.1$  loading using the compression precracking constant amplitude (CPCA) test method (12) show drastically different behavior, as shown in Fig. 2(b), with no “fanning” nor specimen width dependency, as was noted with the E647 LR method. Data for the three specimen widths plotted directly on top of each other over the same range in crack-growth rates examined. The  $\Delta K$ -rate curve is clearly independent of specimen width and crack length, and the rate is only as a function of the applied  $\Delta K$ , a key assumption in the fracture mechanics approach to life prediction. These results indicate that this titanium alloy is very sensitive to load reduction; and caution must be used whenever LR procedures are used. Again, the solid curve in Fig. 2(b) is the predicted behavior for  $R = 0.1$  using the crack-closure model ( $\alpha = 2$ ) and the  $R = 0.7$  data from Ref. 13. In the low- to mid-rate regimes, the rates were over predicted by about 25%.

Newman's crack-closure model (24) was used to correlate  $\Delta K$ -rate data on the three width C(T) specimens to generate the effective stress-intensity factor against rate relation. From past analyses on titanium alloys, a constraint factor ( $\alpha$ ) of 2 had been found to correlate test data over a wide range in stress ratios in the mid-rate regimes. To convert from  $\Delta K$  to  $\Delta K_{\text{eff}}$ , the Elber (25) relation was used

$$\Delta K_{\text{eff}} = (1 - K_o/K_{\text{max}})/(1 - R) \Delta K = U \Delta K \quad (1)$$

where  $K_o$  is the crack-opening stress-intensity factor and  $K_{\text{max}}$  is the maximum value. For low applied stresses and a constraint factor ( $\alpha$ ) of 2, the crack-opening ratio (26, 27) is:

$$K_o/K_{\text{max}} = 0.343 + 0.027 R + 0.917 R^2 - 0.287 R^3 \quad (2)$$

Equation (2) applies for any material that correlates crack-growth-rate data on a  $\Delta K_{\text{eff}}$ -basis with a constraint factor of 2. Figure 2(c) shows all test data using the CPCA test method (13). The data correlated very well over a wide range in stress ratios and specimen widths (28). In these analyses, test data for  $R = 0.7$  was assumed to be closure-free and, thus  $\Delta K = \Delta K_{\text{eff}}$ . The solid curve was a fit to the data shown by symbols. Because there were no data available below a rate of  $1\text{e-}10$  m/cycle, several assumptions were made. First, a  $(\Delta K_{\text{eff}})_{\text{th}}$  value of  $2.5 \text{ MPa}\sqrt{\text{m}}$  was selected (vertical dashed line). Second, a linear extrapolation was made from the lower test data (dashed line) and the lower solid curve is an estimate for small-crack behavior. Small cracks have been shown to grow below the large-crack threshold on a variety of materials. These three extrapolated curves will be used to see how they influence fatigue-life calculations. For high rates, a constraint-loss regime (plane-strain to plane-stress behavior) is expected at a  $(\Delta K_{\text{eff}})_T$  value of about  $38 \text{ MPa}\sqrt{\text{m}}$ . The constraint-loss range was estimated and constraint change was assumed to be linear on log rate (26, 27). Nearly plane-strain ( $\alpha = 2$ ) conditions apply for low rates and plane-stress ( $\alpha = 1$ ) conditions apply for high rates. The elastic fracture toughness,  $K_{\text{Ic}}$ , was  $66 \text{ MPa}\sqrt{\text{m}}$ .

Crack-growth analyses were performed using a multi-linear table-lookup method. The  $\Delta K_{\text{eff}}$ -rate value used in subsequent life analyses was the solid curve with circular symbols, as shown in Figure 2(c). These values are given in Table 1.

## CRACK-CLOSURE MODELING

The crack-closure model (24, 26) was used to calculate crack-opening stresses under constant-amplitude loading to show the influence of an initial defect size on the crack-closure

behavior of small cracks. Previous studies (8-11) have shown that small-crack effects are more pronounced for negative stress ratios.

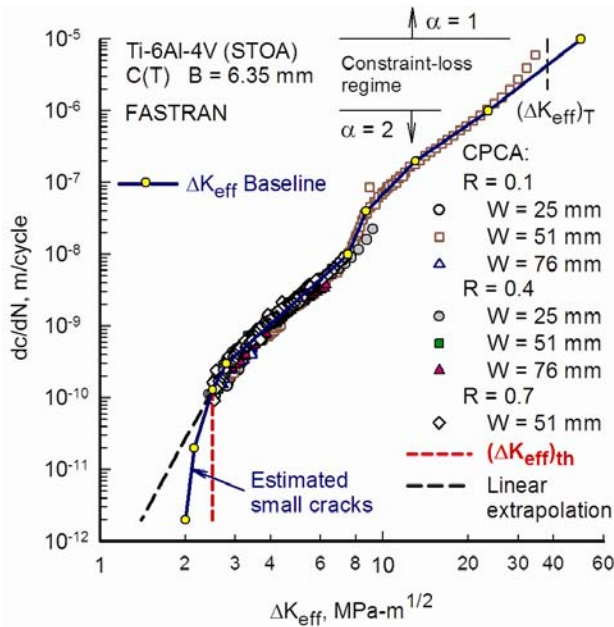


Figure 2(c).  $\Delta K_{\text{eff}}$ -rate data from the CPCA test method and small-crack estimates.

Table 1. Effective stress-intensity factor range against rate relation for small- and large-cracks in Ti-6Al-4V (STOA) alloy.

$\Delta K_{\text{eff}}$ , MPa $\sqrt{\text{m}}$	dc/dN, m/cycle
2.0	2.0e-12
2.15	2.0e-11
2.5	1.3e-10
2.8	3.0e-10
7.5	1.0e-08
8.7	4.0e-08
13.0	2.0e-07
23.5	1.0e-06
50.0	1.0e-05
$\alpha = 2$	$\leq 1.0e-06$
$\alpha = 1$	$\geq 1.0e-05$
$K_{Ie} = 66 \text{ MPa}\sqrt{\text{m}}$	$\sigma_0 = 955 \text{ MPa}$

Some typical results of calculated crack-opening stress-intensity factor ( $K_o$ ) normalized by the maximum applied stress-intensity factor ( $K_{\text{max}}$ ) as a function of surface crack half-length,  $c$ , is shown in Fig. 3. The crack-growth analysis was performed under stress ratios ( $R$ ) of -1, 0.1, 0.5 and 0.8 for a low applied stress (HCF), solid curves, and a high applied stress (LCF), dashed curves, with a constraint factor ( $\alpha$ ) of 2 ( $\alpha = 3$  for plane strain;  $\alpha = 1$  for plane stress). (An unresolved

issue is that a small crack may be acting under plane-stress conditions and not under the high constraint ( $\alpha = 2$ ) conditions assumed in the model and needed for large-crack behavior.) The initial discontinuity ( $a_i = c_i = 12 \mu\text{m}$ ) was assumed to be a void ( $h_n = 6 \mu\text{m}$ ) fully open on the first cycle. As the crack grows into the forward plastic-zone region, crack-opening stresses rapidly builds until the steady-state value for large-crack behavior is approached. The negative stress ratio results show a significant crack-closure transient (due to the assumed void height instead of a tight crack), while the high stress ratio results give crack-opening values as the minimum applied stress-intensity factor (no crack-closure behavior). Herein, the initial  $a_i/c_i$  ratio was assumed to be unity; and the initial void height,  $h_n$ , was assumed to be one-half of  $a_i$  (or  $c_i$ ).

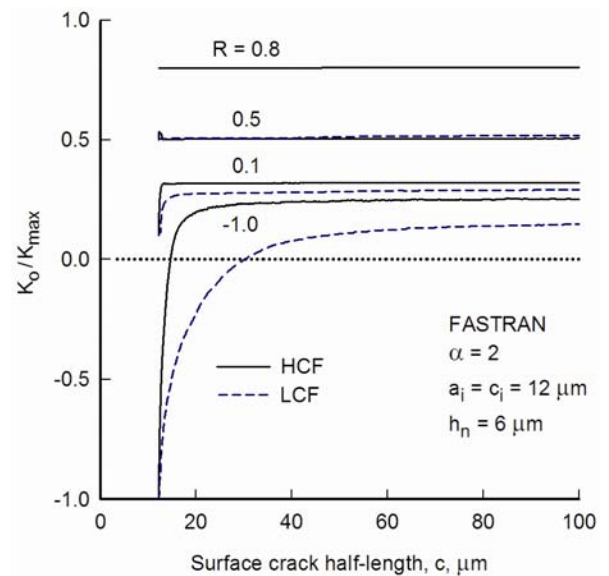


Figure 3. Crack-closure behavior for small cracks under low- and high-stress levels.

The J-integral is one of the most commonly used parameters for non-linear crack-growth analyses. El Haddad et al. (29) and Hudak and Chan (30) have made  $\Delta J$  estimates for small cracks. Because crack-closure effects may be one of the key elements in small-crack growth,  $\Delta J$  should be computed using only that portion of the load cycle during which the crack is fully open (or  $\Delta J_{\text{eff}}$ ). Modifications to account for crack-closure effects are discussed later. To develop a non-linear crack-tip parameter for small cracks, it is convenient to define an equivalent plastic stress-intensity factor  $K_J$ , in terms of the J-integral, as

$$K_J^2 = JE/(1-\eta^2) = \sigma_0 \delta E/(1-\eta^2) \quad (3)$$

where  $E$  is the modulus,  $\eta = 0$  for plane stress,  $\eta = \nu$  (Poisson's ratio) for plane strain,  $\sigma_0$  is the flow stress, and  $\delta$  is the crack-tip-opening displacement. As shown by Rice (31) from the Dugdale model, the J-integral is equal to  $\sigma_0 \delta$ . A common

practice in elastic-plastic fracture mechanics has been to add a portion of the plastic-zone size ( $\rho$ ) to the crack length to account for crack-tip yielding. An estimate for  $J$  was determined in Ref. 32 by first defining a plastic-zone-corrected stress-intensity factor as

$$K_p = S \sqrt{(\pi d)} F(d/w, d/r, \dots) \quad (4)$$

where  $d = c + \gamma\rho$ ,  $F$  is the boundary-correction factor,  $w$  is specimen width and  $r$  is hole radius. The term  $\gamma$  was assumed to be a constant and was evaluated by equating  $K_p$  to  $K_I$  for several cracked bodies (32). A value of 1/4 was found to give good agreement between  $K_p$  and  $K_I$  up to large values of applied stress to flow stress ( $S/\sigma_o$ ) ratios and  $\rho/a$  up to 100.

Elber's effective stress-intensity factor range (25) was based on linear-elastic analyses. To account for plasticity, a portion of the Dugdale cyclic-plastic-zone length ( $\omega$ ) has been added to the crack length. Thus, the cyclic-plastic-zone-corrected effective stress-intensity factor range is:

$$(\Delta K_p)_{\text{eff}} = (S_{\text{max}} - S_o) \sqrt{(\pi d)} F(d/w, d/r, \dots) \quad (5)$$

where  $S_{\text{max}}$  is the maximum stress,  $S_o$  is the crack-opening stress,  $d = c + \gamma\omega$  and  $F$  is the boundary-correction factor. For large-crack behavior, the cyclic-plastic-zone correction was found to be insignificant. For small cracks emanating from a hole or notch, the cyclic-plastic-zone corrected stress-intensity factor was found to be very significant for applied stress levels greater than about one-half of the flow stress of the material.

### SMALL- AND LARGE-CRACK BEHAVIOR

Small- and large-crack data was obtained on the titanium alloy in the USAF report (17-21) at room temperature and lab-air conditions at several stress ratios. The large-crack data was obtained from standard compact C(T) specimens (6.35 mm thick;  $w = 51$  mm), and the scatter band for the  $R = 0.1$  data (18) is shown in Fig. 4(a). (All test data and curves are  $\Delta K$  values unless noted as  $\Delta K_{\text{eff}}$ .) The small-crack data (open circles) was obtained from circular rods (5 mm diameter) using the replica method employing acetyl cellulose film (19). Small cracks initiated as surface cracks growing at the free surface of the rods and they were assumed to be semi-circular surface cracks (19). Various reports (17, 33, 34) also discuss the possibility that some of the surface cracks may have initiated as sub-surface embedded cracks. And the small-crack data showed a pronounced small-crack effect that will be discussed later.

In Fig. 4(a), the solid lines with circular symbols are the  $\Delta K_{\text{eff}}$ -rate baseline relation determined from C(T) specimens in Fig. 2(c) with data from Ref. 13. Again, the lower dashed lines with circular symbols are the estimated behavior for small cracks. The solid and dashed lines are the predicted and estimated behavior for  $R = 0.1$  loading, which agreed well for rates greater than about  $1e-9$  m/cycle. But the large-crack data from the USAF report (17, 18) is approaching a higher

threshold than the predicted curve because of load-history effects from load shedding, similar to that shown in Fig. 2(a).

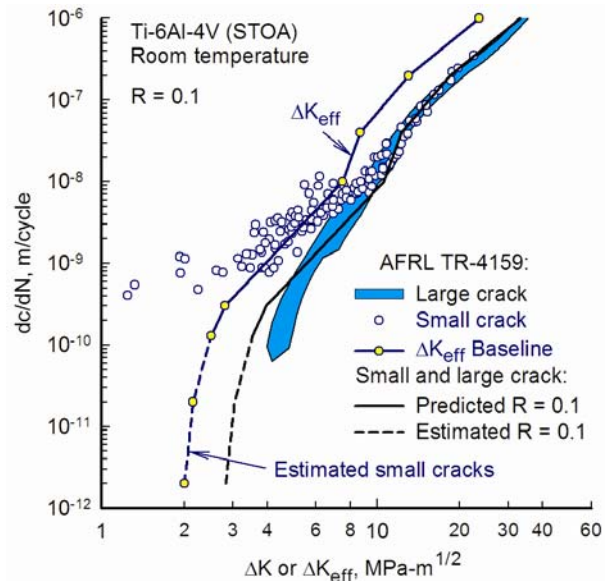


**Figure 4(a). Small- and large-crack-growth-rate data with LEM and closure-based relations at  $R = 0.1$ .**

Small-crack data from the USAF report (17, 19) for  $R = 0.5$  loading are shown as square open symbols in Fig. 4(b). Again, the small cracks were assumed to be semi-circular surface cracks, but some of these cracks may have initiated as sub-surface embedded cracks. These small-crack data also show some pronounced small-crack effects for low values of  $\Delta K$ . The  $\Delta K_{\text{eff}}$ -rate curve (solid and dashed lines with symbols) and the predicted behavior for  $R = 0.5$  and  $-1$  loading are shown as solid and dashed lines. At  $R = 0.5$  and  $\Delta K$  values greater than about  $3 \text{ MPa}\sqrt{\text{m}}$ , the small- and large-surface-crack data agreed fairly well with the predicted large-crack results from C(T) specimens, except at the very high rates. Also, the triangular symbols are test data on middle-crack tension specimens on a mill-annealed titanium alloy (35). Again, the test data agreed fairly well with the predicted behavior at  $R = -1$ , except the mill-annealed alloy did not show a sharp transition in the mid-region.

In an effort to try to explain the pronounced small-crack effects shown in Figs. 4(a) and 4(b), some measured rates on small cracks in the round-bar specimens (19, 33, 34) are shown in Fig. 5. Here crack-growth rate is plotted against the surface crack half-length,  $c$ . Five tests were conducted at a maximum stress level of  $613 \text{ MPa}$  at  $R = 0.1$ , as shown by the solid curves with symbols. The fatigue lives for these tests ranged from 1.6 to 3 million cycles with an average of 2.1 million cycles. The measured results show an extremely high initial rate followed by a rapid drop and a slow rise at longer crack lengths. These small-crack effects could not be explained from crack-closure transients nor plasticity effects at  $R = 0.1$ .

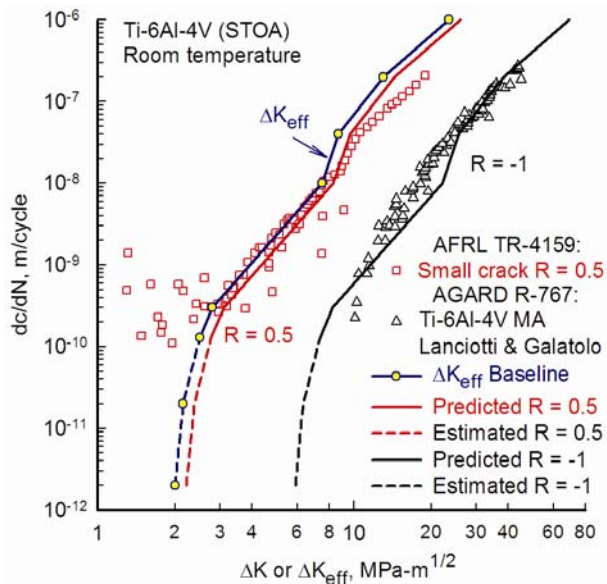


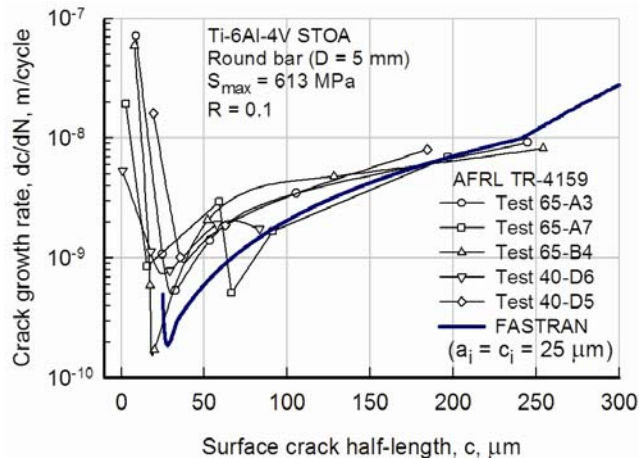
**Figure 4(b). Small- and large-crack-growth-rate data with LEFM and closure-based relations at  $R = 0.5$  and  $-1$ .**

For the  $K_T = 1$  specimens, a large amount of scatter was observed at this particular stress level (16, 19, 20). Fatigue lives ranged from 140,000 to about 5 million cycles. The reason for the large amount of scatter was also not known.

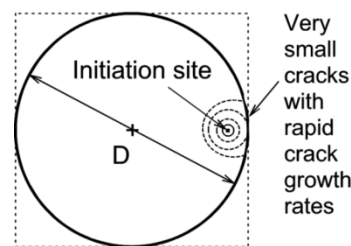
FASTRAN [26] with a 25- $\mu\text{m}$  (initial semi-circular surface crack) and the  $\Delta K_{\text{eff}}$ -rate curve (Table 1), predicted about 150,000 cycles to failure. (Reason for selecting the 25- $\mu\text{m}$  flaw will be discussed later.) This life, however, agreed fairly well with the lower bound of the fatigue tests. The solid curve in Fig. 5 is the predicted results from the life-prediction code. It shows a slight drop in the initial stages and followed by a slow rise at larger crack lengths, similar to the test data. But the code still predicted slower rates than measured from the small-crack tests. (FASTRAN Version 5.33 was used herein.)

Since various reports (16, 19, 33, 34) have discussed the possibility of sub-surface crack initiation sites, the extremely high rates at very small crack lengths may be explained by Fig. 6. The crack at a sub-surface initiation site will grow as a fish-eye crack under vacuum. When the near circular crack penetrates the free surface, the observed crack length could be very small, but the stress-intensity factor would be very large due to the vertex at the crack front (34). This could explain the very rapid crack-growth rates at very small crack lengths.

The sub-surface initiation sites could also help explain the large differences in the fatigue life scatter observed at this particular stress level. Fatigue cracks grow much slower in vacuum than lab-air, so several million cycles could elapse before the crack penetrates the free surface. This could also explain why the USAF report stated that the "crack propagation life was very small compared to the total fatigue life".



**Figure 5. Measured and calculated small-crack growth in round bar under constant-amplitude loading.**



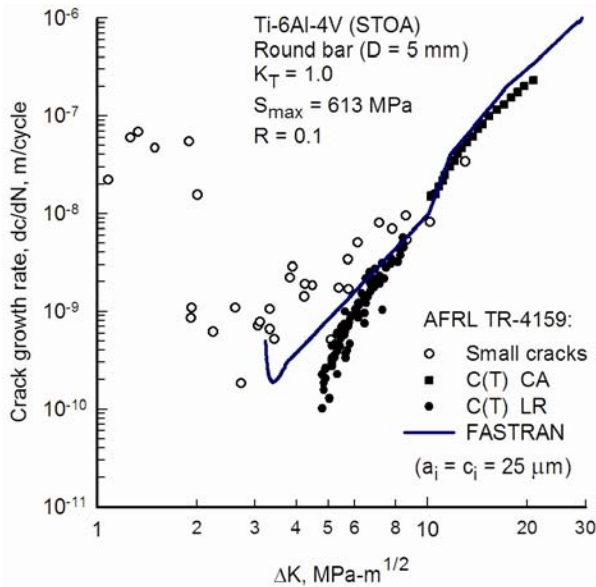
**Figure 6. Assumed sub-surface initiation site (fish-eye) with extremely high rates observed at free-surface crack penetrating location.**

Figure 7 shows the  $\Delta K$ -rate results on the small-crack data from the round-bar specimens and large-crack data on C(T) specimens (18-20). Square symbols are C(T) tests at  $R = 0.1$  constant-amplitude loading, which agree very well with the FASTRAN calculations for large cracks. The solid circular symbols are C(T) tests conducted using the ASTM load-shedding method, which produced an elevated threshold and slower rates in the near-threshold regime. FASTRAN calculations produced faster rates and crack growth at lower  $\Delta K$  values than the load-shedding test data. Further study is required to determine whether the sub-surface initiation sites, modified stress-intensity factor solutions, and vacuum crack growth are the reasons for the unusual small-crack effects observed in these tests.

## FATIGUE-LIFE CALCULATIONS

Small-crack theory and equivalent initial flaw sizes (EIFS) have been used to calculate the fatigue lives on three types of fatigue tests. Small-crack theory is the use of measured small-crack data and the non-linear crack-closure model to calculate or predict the fatigue life of smooth and notched specimens or components. Herein, crack growth in the  $a$ - and  $c$ -directions was assumed to be equal (i.e.,  $\Delta K_{\text{eff}}-da/dN$  and  $\Delta K_{\text{eff}}-dc/dN$  relations were the same). The fatigue test data were obtained

from either the USAF HCF report (17-21) or the Metallic Materials Properties Development Standards Handbook (22). All tests were subjected to constant-amplitude loading over a wide range of stress levels and stress ratios. First, smooth ( $K_T = 1$ ) flat sheets or round-bar specimens were analyzed. Second, fatigue tests on circular hole ( $K_T = 3$ ) flat sheet specimens were compared with the calculated results. And last, double-edge-notch ( $K_T = 3.06$ ) specimens were analyzed.



**Figure 7. Measured and calculated small- and large-crack-growth rates at  $R = 0.1$ .**

**Smooth ( $K_T = 1$ ) Specimens**

Figure 8 shows fatigue tests conducted on round bars ( $D = 4$  to  $5$  mm) that had been polished and these data were obtained from the USAF report (17, 19). The maximum stress level is plotted against the fatigue life. Fatigue tests were conducted by three different organizations (open symbols) and the solid symbols are fatigue lives from cyclic stress-strain tests (16). The diamond symbol and scatter band shows the fatigue tests (19, 33, 34) that were used to measure small-crack growth rates, as shown in Figs. 5 and 7. If small-crack tests and measurements had been made on some of the shorter fatigue-life tests, which may have resulted in surface initiation sites, then a much different small-crack effect may have been seen from these tests.

In the FASTRAN analyses, a  $25\text{-}\mu\text{m}$  semi-circular surface crack was assumed as the initial flaw in a square bar (see dashed line insert in Fig. 6), since the stress-intensity factor solution for a surface crack in a round bar was not available in the life-prediction code (26). (Since the majority of the fatigue life is spent as a micro-structurally small crack, the difference between a square- or round-bar would not be significant.) The calculated fatigue lives (solid curve) agreed very well with the test data at the higher stress levels, but underestimated the endurance limit. At very high applied stress levels, the life-

prediction model predicts failure when the applied stress is nearly equal to the flow stress ( $\sigma_0$ ) of the material.

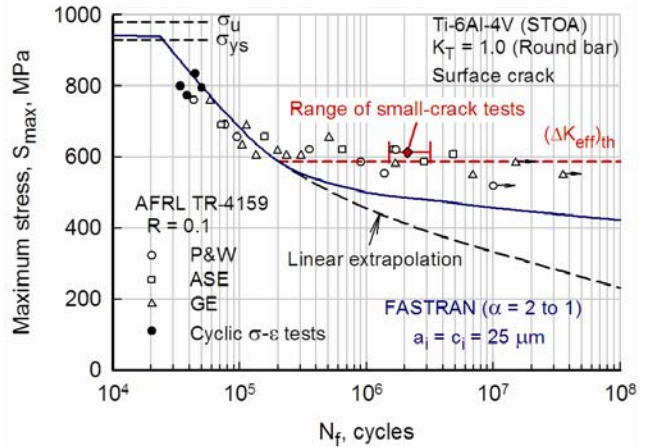


**Figure 8. Stress-life and calculated behavior for round bar with  $K_T = 1$ .**

Using the linear extrapolated curve in Fig. 2(c) and the  $25\text{-}\mu\text{m}$  flaw, the calculated fatigue lives fell very short for low applied stress levels, but matched the test data for applied stresses greater than about  $600$  MPa. The separation point between the solid and dashed curves is at a rate of about  $1\text{e-}10$  m/cycle. But using an effective threshold,  $(\Delta K_{eff})_{th}$ , of  $2.5$  MPa $\sqrt{\text{m}}$  matched the test data quite well with a  $25\text{-}\mu\text{m}$  flaw. However, the solid curve in Fig. 2(c) will be used for further fatigue-life calculations because the long-life tests are suspected to have been initiated as sub-surface flaws, as previously stated.

Figure 9 shows fatigue tests conducted on flat rectangular sheets ( $w = 25.4$  mm;  $B = 1.6$  or  $3.2$  mm) that had been polished and cleaned. These test data were obtained from Ref. 22. Again, the maximum applied stress,  $S_{max}$ , is plotted against the fatigue life. Tests were conducted at  $R = -1, 0$  or  $0.05$  and  $0.54$  over a wide range in remote applied stress levels.

In the FASTRAN analyses, a corner crack in a sheet was assumed as the initial flaw. A trial-and-error method was used to find an initial quarter-circular crack that would result in reasonable life calculations for the  $R = -1$  test conditions. Again, a  $25\text{-}\mu\text{m}$  flaw produced reasonable calculated fatigue lives for most of the stress levels (lower solid curve), and matched the endurance limit for the  $R = -1$  tests quite well. Using the same initial flaw size for the  $R = 0$  and  $0.54$  loading, produced reasonable lives at the higher stress levels and matched the endurance limit for the high  $R$  tests, but underestimated the endurance limit for the  $R = 0$  tests, similar to the results in Fig. 8. The upper failure stress for all  $R$  ratios was very near to the flow stress of the material.

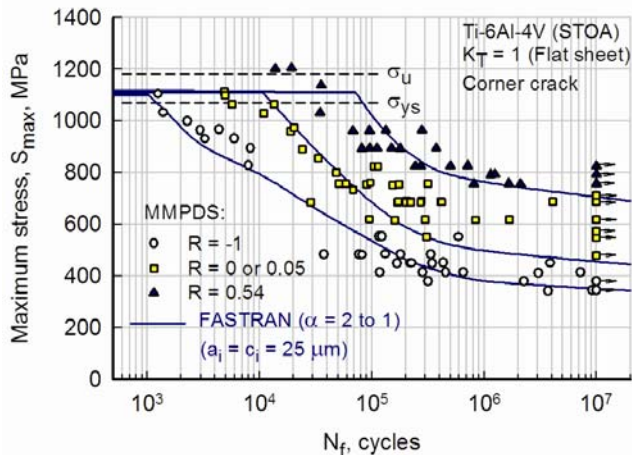


**Figure 9. Stress-life and calculated behavior for flat sheet with  $K_T = 1$ .**

The existence of a 25- $\mu\text{m}$  initial flaw early in the fatigue life on the  $K_T = 1$  specimens may be unreasonable, since the average grain size is only about 20- $\mu\text{m}$  (16). It may be that the estimated  $\Delta K_{\text{eff}}$ -rate curve in Fig. 2(c) is still not correct, the state-of-stress for small cracks is more like plane stress ( $\alpha = 1$  to 1.1) instead of plane strain ( $\alpha = 2$ ), and/or the influence of the microstructural grain orientation on crack-closure behavior is needed. However, the answers to these questions may have to wait for more small-crack data, since the small-crack tests in the USAF report (16, 19) had some concerns about sub-surface initiation sites and improper stress-intensity factor solutions for a free surface penetrating crack (see Fig. 6). In addition, crack-closure measurements on small cracks at both positive and negative stress ratios are needed and more elastic-plastic stress analyses on the early stages of small-crack growth in the proper microstructure could lead to a better understanding.

### Circular Hole ( $K_T = 3$ ) Specimens

Figure 10 shows fatigue tests conducted on flat rectangular sheets ( $w = 25.4$  mm;  $B = 1.6$  or  $3.2$  mm) containing a central circular hole ( $D = 1.6$  mm) that had been polished and cleaned. These test data were obtained from Ref 22. Here the maximum applied gross stress,  $S_{\text{max}}$ , is plotted against the fatigue life, instead of the net-section stress. Tests were conducted at  $R = -1$ , 0 and 0.54 over a wide range in remote applied stress levels.

In the FASTRAN analyses, a single surface crack at the center of the circular hole was assumed as the initial flaw. Again, a trial-and-error method was used to find an initial crack size that would result in reasonable life calculations for  $R = -1$  test conditions. A 6- $\mu\text{m}$  semi-circular flaw produced reasonable calculated fatigue lives (solid curve) for all of the stress levels, and even matched the endurance limit very well. Using the same initial flaw size for the  $R = 0$  and 0.54 loading, reasonable fatigue lives were calculated at all stress levels with a slight over estimations on the long lives for the high- $R$  tests.

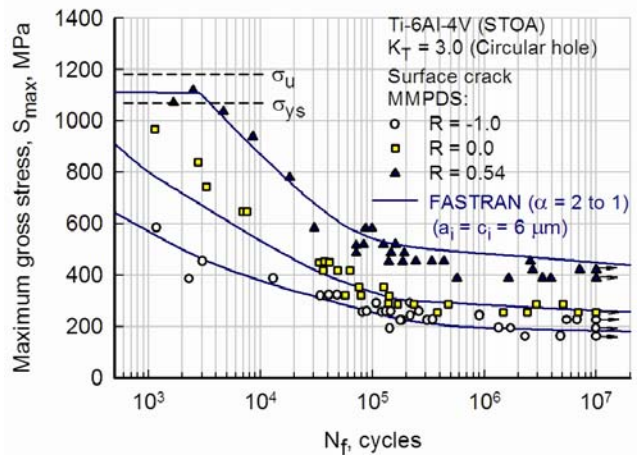


**Figure 10. Stress-life and calculated behavior for flat sheet with  $K_T = 3$ .**

The smaller initial flaw size for the circular-hole specimens are reasonable, since a much smaller volume of material is being subjected to the high stress level around the hole. For the un-notched ( $K_T = 1$ ) specimens, a much larger volume of material is subjected to the applied stress and the presence of a larger flaw may be the initiation site. Thus, the un-notched specimens may be more likely to have sub-surface initiation sites than the circular-hole specimens.

### Double-Edge Notch ( $K_T = 3.06$ ) Specimens

Figures 11(a) and 11(b) show fatigue tests conducted on double-edge-notched specimens with a  $K_T = 3.06$  (based on gross applied stress) that were obtained from the USAF report (16, 21). The maximum gross stress level,  $S_{\text{max}}$ , is plotted against the fatigue life for tests conducted at a stress ratio of  $R = -1, 0.1, 0.5$  and  $0.8$ .

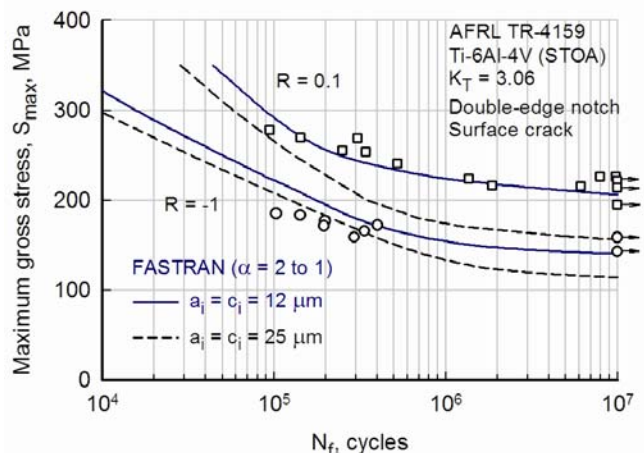


**Figure 11(a). Stress-life and calculated behavior for double-edge-notch specimens with  $K_T = 3.06$  at  $R = -1$  and  $0.1$ .**

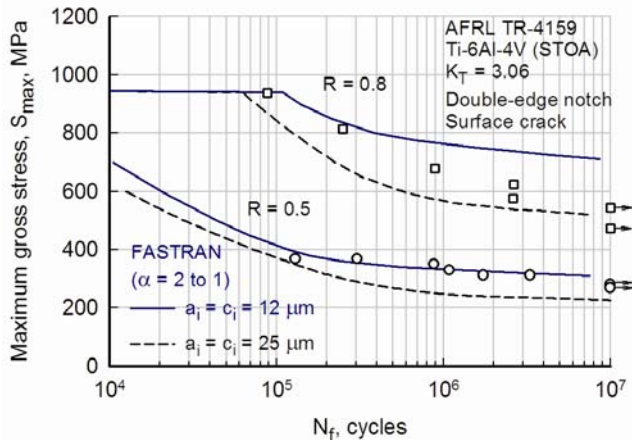


**Figure 11(b). Stress-life and calculated behavior for double-edge-notch specimens with  $K_T = 3.06$  at  $R = 0.5$  and  $0.8$ .**

In the FASTRAN analyses, a surface crack located at the center of one semi-circular edge notch was considered with a total width of  $2w$  (see Fig. 1(c)), since the double-edge-notch configuration is not in the current life-prediction code. Thus, the adjacent edge notch was not considered in the stress-intensity factor solution. This assumption is satisfactory because most of the fatigue life is consumed in the small-crack regime. Of course, the stress-concentration factor accounted for the presence of the double notches and the stress-intensity factor solution for a surface crack is influenced by the local stress-concentration factor.

In Figs. 11(a) and 11(b), the fatigue-life calculations have been made for semi-circular surface cracks of 12- and 25- $\mu\text{m}$ . The 25- $\mu\text{m}$  flaw fit the  $R = -1$  test data fairly well. Whereas, the 12- $\mu\text{m}$  flaws fit the test results for the  $R = 0$  and 0.5 loading conditions. And the 12- and 25- $\mu\text{m}$  flaw bounded the test results for  $R = 0.8$  loading.

## CONCLUDING REMARKS

Small-crack theory and equivalent-initial-flaw-sizes (EIFS) were used to calculate fatigue lives (stress-life) for notched and un-notched specimens made of a Ti-6Al-4V (STOA) alloy and tested at room temperature and laboratory-air conditions. Smooth specimens (flat sheet and round bars), flat sheet with circular holes and double-edge-notched plates were analyzed. The following conclusions were found:

(1) For large cracks, the load-reduction test method caused elevated thresholds and slower crack-growth rates than the compression precracking constant-amplitude (CPCA) test method.

(2) Plasticity effects on the effective stress-intensity factor range were small, even for very high applied stress levels, but the crack-closure transients appeared to be the dominate mechanism for rapid small-crack growth.

(3) Using FASTRAN (constraint factor,  $\alpha = 2$ ) and small-crack theory, smooth ( $K_T = 1$ ) fatigue specimens produced an EIFS (surface or corner cracks) of 25- $\mu\text{m}$  for moderate to high applied stress levels at  $R = -1$  to 0.54, but under estimated the endurance limits at  $R = 0$  or 0.1. Sub-surface crack initiation sites may have been the reason for the higher endurance limits.

(4) Using FASTRAN (constraint factor,  $\alpha = 2$ ) and small-crack theory, notched ( $K_T = 3$  or 3.06) fatigue specimens produced an EIFS (surface cracks) from 6 to 12- $\mu\text{m}$  for positive stress ratios ( $R = 0$  and 0.54), and 25- $\mu\text{m}$  for negative stress ratio ( $R = -1$ ) loading.

## ACKNOWLEDGMENTS

Authors thank the U. S. Air Force Research Laboratories (AFRL) for the fatigue test data on the titanium alloy; and Pratt & Whitney for financial support of this research effort.

## REFERENCES

- (1) Pearson, S., 1975, "Initiation of Fatigue Cracks in Commercial Aluminum Alloys and the Subsequent Propagation of Very Short Cracks," *Engineering Fracture Mechanics*, Vol. 7, pp. 235-247.
- (2) Kitagawa, H., and Takahashi, S., 1976, "Applicability of Fracture Mechanics to Very Small Cracks or the Behaviour in the Early Stages," *Proceedings Second International Conference on Mechanical Behavior of Materials*, Boston, MA, pp. 627-631.
- (3) Zocher, H., ed., 1983, "*Behaviour of Short Cracks in Airframe Components*," AGARD CP-328.
- (4) Ritchie, R. O., and Lankford, J., eds., 1986, "Small Fatigue Cracks," The Metallurgical Society, Inc., Warrendale, PA.
- (5) Miller, K. J., and de los Rios, E. R., eds., 1986, "The Behaviour of Short Fatigue Cracks," *European Group on Fracture*, Publication No. 1.
- (6) Ritchie, R. O., and Lankford, J., 1986, "Overview of the Small Crack Problem", Small Fatigue Cracks, R. O. Ritchie and J. Lankford, eds., pp. 1-5.
- (7) Newman, J. C., Jr., 1983, "A Nonlinear Fracture Mechanics Approach to the Growth of Small Cracks," *Behaviour of Short Cracks in Airframe Components*, Zocher, H., ed., AGARD CP-328, pp. 6.1-6.26.
- (8) Newman, J. C., Jr., Swain, M. H. and Phillips, E. P., 1986, "An Assessment of the Small-Crack Effect for 2024-T3 Aluminum Alloy," Small Fatigue Cracks, The Metallurgical Society, Inc., Warrendale, PA, pp. 427-452.
- (9) Newman, J. C., Jr., and Edwards, P. R., 1988, "Short-Crack Growth Behaviour in an Aluminum Alloy - an AGARD Cooperative Test Programme," AGARD R-732.
- (10) Newman, J. C., Jr., Phillips, E. P. and Swain, M. H., 1997, "Fatigue-Life Prediction Methodology using Small-Crack Theory," NASA TM-110307.

- (11) Newman, J. C., Jr., Phillips, E. P. and Everett, R. A., Jr., 1999, "Fatigue Analyses under Constant- and Variable-Amplitude Loading using Small-Crack Theory," NASA TM-209329.
- (12) Newman, J. C., Jr., Schneider, J., Daniel, A., and McKnight, D., 2005, "Compression Pre-cracking to Generate near Threshold Fatigue-Crack-Growth Rates in Two Aluminum Alloys," *International Journal of Fatigue*, Vol. 27, p. 1432.
- (13) Ruschau, J. J., and Newman, J. C., Jr., 2008, "Compression Precracking to Generate Near Threshold Fatigue-Crack-Growth Rates in an Aluminum and Titanium Alloy," *Journal of ASTM International*, Vol. 5, No.7.
- (14) Yamada, Y., and Newman, J. C., Jr., 2009, "Crack Closure under High Load-Ratio Conditions for Inconel-718 Near Threshold Conditions," *Engineering Fracture Mechanics*, Vol. 76, pp. 209-220.
- (15) Suresh, S., "Crack Initiation in Cyclic Compression and Its Application," *Engineering Fracture Mechanics*, Vol. 21, 1985, pp. 453-463.
- (16) Pippan, R., Plöchl, L., Klanner, F., and Stüwe, H. P., 1994, "The Use of Fatigue Specimens Precracked in Compression for Measuring Threshold Values and Crack Growth," *ASTM Journal of Testing and Evaluation*, Vol. 22, p. 98.
- (17) Gallagher, J. P. et al., 2001, "Improved High-Cycle Fatigue (HCF) Life Prediction," AFRL-ML-WP-TR-2001-4159.
- (18) deLaneville, R. E. and Sheldon, J. W., "Crack Growth," AFRL-ML-WP-TR-2001-4159, Appendix 3B, 2001, pp. 1-12.
- (19) Lenets, Y. N., "Nucleation and Propagation of Small Cracks," AFRL-ML-WP-TR-2001-4159, Appendix 3C, 2001, pp. 1-14.
- (20) Bellows, R., "Effect of Specimen Geometry and Frequency on HCF Smooth Specimen Behavior," AFRL-ML-WP-TR-2001-4159, Appendix 3F, 2001, pp. 1-4.
- (21) deLaneville, R. E. and Sheldon, J. W., "Notch Fatigue," AFRL-ML-WP-TR-2001-4159, Appendix 3J, 2001, pp. 1-6.
- (22) Metallic Materials Properties Development and Standardization, U.S. Department of Transportation, Federal Aviation Administration, DOT/FAA/AR-MMPDS-01, 2003, Washington, D.C.
- (23) Garr, K. R., and Hresko, G. C., 2000, "A Size Effect on the Fatigue Crack Growth Rate Threshold of Alloy 718," *ASTM STP 1372*, West Conshohocken, PA, pp. 155-174.
- (24) Newman, J. C., Jr., 1981, "A Crack Closure Model for Predicting Fatigue Crack Growth under Aircraft Spectrum Loading," *ASTM STP 748*, pp. 53-84.
- (25) Elber, W., 1971, "The Significance of Fatigue Crack Closure," *ASTM STP 486*, pp. 230-242.
- (26) Newman, J. C., Jr., 1992, "FASTRAN-II - A Fatigue Crack Growth Structural Analysis Program," NASA TM 104159.
- (27) Newman, J. C., Jr., "Effects of Constraint on Crack Growth under Aircraft Spectrum Loading," *Fatigue of Aircraft Materials*, A. Beukers et al, Eds., Delft University Press, 1992, pp. 83-109.
- (28) Newman, J. C., Jr., Ruschau, J. J., and Hill, M. R., "Improved Test Method for Very Low Fatigue-Crack-Growth-Rate Data," *Fatigue and Fracture of Engineering Materials and Structures*, accepted August 2010.
- (29) El Haddad, M. H., Dowling, N. E., Topper, T. H., and Smith, K. N., 1980, "J-Integral Application for Short Fatigue Cracks at Notches," *International Journal of Fracture*, Vol. 16, pp. 15-30.
- (30) Hudak, S. J., Jr., and Chan, K. S., 1986, "In Search of a Driving Force to Characterize the Kinetics of Small Crack Growth," *Small Fatigue Cracks*, R. O. Ritchie and J. Lankford, eds., Metallurgical Society, pp. 379-405.
- (31) Rice, J. R., 1968, "A Path Independent Integral and the Approximate Analysis of Strain Concentration by Notches and Cracks," *Journal of Applied Mechanics*, Vol. 35, pp. 379-386.
- (32) Newman, J. C., Jr., 1992, "Fracture Mechanics Parameters for Small Fatigue Cracks," *ASTM STP 1149*, pp. 6-28.
- (33) Lenets, Y. N., Bellows, R. and Merrick, H., "Propagation Behavior of Naturally Initiated Cracks in Round Bars of Ti-6Al-4V, Proceedings of 5<sup>th</sup> National Turbine High Cycle Fatigue Conference, HCF'00, 2000.
- (34) Lenets, Y. N., Nelson, R. and Merrick, H., "Growth of Small Cracks at Different Stress Ratios," Proceedings of 7<sup>th</sup> National Turbine Engine High Cycle Fatigue Conference, HCF'02, 2002.
- (35) Lanciotti, A., and Galatolo, R., "Short Crack Observations in Ti-6Al-4V under Constant Amplitude Loading," AGARD R-732, pp. 10.1-10.7.